A Letters Journal Exploring the Frontiers of Physics

February 2020

EPL, **129** (2020) 37004
doi: 10.1209/0295-5075/129/37004

www.epljournal.org

The origin of weak coupling between polar clusters in Ta_2O_5-doped $0.94Bi_{0.5}Na_{0.5}TiO_3$-$0.06BaTiO_3$

Xiafeng He[1], Shuo Zhou[1], Zhi Yuan[2], Yunhua Li[3], Zhencheng Lan[1], Kaiyuan Chen[1], Feifei Han[1], Xiuyun Lei[1] and Laijun Liu[1(a)]

[1] *Guangxi Key Lab of Optical and Electronic Functional Materials and Devices, College of Materials Science and Engineering, Guilin University of Technology - Guilin 541004, China*
[2] *College of Energy and Building Environment, Guilin University of Aerospace Technology - Guilin 541000, Guangxi, China*
[3] *College of Mechanical and Electronic Engineering, Jiangxi College of Applied Technology - Ganzhou, 341004, Jiangxi, China*

received 10 November 2019; accepted in final form 12 February 2020
published online 2 March 2020

PACS 77.84.-s – Dielectric, piezoelectric, ferroelectric, and antiferroelectric materials
PACS 77.80.Jk – Relaxor ferroelectrics

Abstract – Ta_2O_5-doped $0.94Bi_{0.5}Na_{0.5}TiO_3$-$0.06BaTiO_3$ [$(1-x)$(0.94BNT-0.06BT)-xTa (x = 0.00–0.02)] ceramics were prepared by a solid-state reaction technique. The single perovskite structure with space group $R3c$ of the ceramics was identified by X-ray diffraction (XRD). Raman spectroscopy revealed the evolution of the local structure with Ta_2O_5 concentration. The temperature dependence of dielectric permittivity of the ceramics were deconvoluted by three Gaussian distribution functions which suggests that three dielectric anomalies exist in this system. The low-temperature dielectric anomaly exhibits a typical relaxor behavior with strong frequency dispersion (reentrant relaxor behavior). The activation energy derived from the V-F law is 0.298 eV, 0.338 eV, 0.412 eV and 0.449 eV, for x = 0.00, 0.005, 0.01 and 0.02, respectively. The mid-temperature and high-temperature anomalies are attributed to two structure phase transitions. The increase of the activation energies suggests that the coupling between polar clusters or polar nanoregions (PNRs) becomes weaker. The origin of the interaction between PNRs and phase transition behavior has been proposed according to the average structure, local structure and defect compensation mechanism of the system.

Introduction. – The most widely used piezoelectric and ferroelectric ceramics are lead-based $PbZrO_3$-$PbTiO_3$ (PZT) multi-component systems around the morphotropic phase boundary (MPB) because of their high standard and distinguished electromechanical properties [1–5]. However, these lead-based materials have caused serious damage to the environment during the process of production at high temperature or post-treatment after usage. Thus, it is urgent to develop high-performance lead-free piezoelectric ceramics to replace PZT-based ceramics.

$Bi_{0.5}Na_{0.5}TiO_3$(BNT)-based ceramics show distinguished piezoelectric and ferroelectric properties as lead-free candidate material. As a hopeful candidate, BNT has a high Curie temperature (T_c = 320 °C) and relatively large remnant polarization (P_r = 38 μC/cm^2) [6]. However, pure BNT is very hard to be polarized because of its relatively large conductivity and high coercive field (E_c = 7.3 kV/mm). To solve this problem, many BNT-based solid solutions, such as BNT-$Bi_{1/2}K_{1/2}TiO_3$-$K_{0.5}Na_{0.5}NbO_3$ [7], BNT-$Bi_{0.5}K_{0.5}TiO_3$-$BaTiO_3$ [8], BNT-$BaTiO_3$-$K_{0.5}Na_{0.5}NbO_3$ [9–11] have been developed in the past several years. Among these developed ceramics, $0.94Bi_{0.5}Na_{0.5}TiO_3$-$0.06BaTiO_3$ (0.94BNT-0.06BT) system reflects excellent electrical properties owing to the existence of MPB as starting point of lead-free materials development [12,13]. In order to enhance the properties of lead-free piezoelectric ceramics, rare earth oxides are often used as a dopant. For example, 0.94BNT-0.06BT ceramics doped with Y_2O_3 cause the ceramics of ferroelectric domains easier reorientation during the polarization process, which leads to an improvement in piezoelectric properties [14]. 0.94BNT-0.06BT ceramics doped with

(a)E-mail: ljliu2@163.com

3 mol% Yb_2O_3 display near platform dielectric behavior in a broad temperature range with low dielectric loss [15]. The ceramics 0.94BNT-0.06BT doped with CeO_2 and Ga_2O_3 show high piezoelectric properties and low dissipation factor [16,17]. 0.94BNT-0.06BT ceramics doped with 0.3 wt.% Sm_2O_3, 0.25 wt.% Eu_2O_3 and 0.4 wt.% Nd_2O_3 show excellent piezoelectric properties in 0.94BNT-0.06BT [18–20].

However, the role of doped ions on the local structure and dielectric responses of 0.94BNT-0.06BT is not clear. In addition, the evaporation of bismuth and sodium usually creates oxygen vacancies and then gives rise to high conductivity in the BNT-based system, which has a negative effect on the application as capacitors. Therefore, in this paper, tantalum was selected as a donor to restrict the concentration of oxygen vacancies in 0.94BNT-0.06BT ceramics. More important, the local structures of the ceramics with the concentration of tantalum were characterized by Raman spectroscopy. The dielectric relaxation model was employed to describe the dielectric response associated with different response mechanisms at selected temperatures. The relationship between local structure transition and dielectric response was constructed in order to give insight into the mechanism of weak coupling between polar clusters or PNRs.

Experimental procedure. – $(1-x)(0.94Bi_{0.5}Na_{0.5}TiO_3\text{-}0.06BaTiO_3)$-$x$Ta ($x$ = 0.00, 0.005, 0.01, 0.02) ceramics were prepared by using a conventional solid-state reaction process, as reported in our previous work [15]. The raw materials Bi_2O_3 (99.9%), Ta_2O_5 (99.99%), TiO_2 (99.99%), $BaCO_3$ (99.9%) and Na_2CO_3 (99.8%) were high-purity oxides and carbonates. These samples were sintered at 1100–1200 °C in air for 2 h.

The crystal structure of the ceramics was determined by X-ray diffraction (X'Pert PRO, PANalytical) using Cu $K\alpha$ radiation ($\lambda = 1.5406$ Å). A DXR microscopy Raman spectrometer (Thermo Fisher Scientific Co.) was used to record Raman spectroscopy. Dielectric properties of the samples were measured by connecting an impedance analyzer (Agilent 4294 A, Hyogo, Japan) to a tube furnace with controlled temperature.

Results and discussion. – The Rietveld refinement of XRD patterns for the $(1-x)$(0.94BNT-0.06BT)-xTa ceramics using FULLPROF software is shown in fig. 1. All sintered samples have a pure perovskite structure, indicating that Ta diffuses into the lattice of 0.94BNT-0.06BT. The structure of the 0.94BNT-0.06BT ceramics performs a rhombohedral symmetry with space group $R3c$ because the tetragonal distortion ($P4bm$) could not be detected [21]. The obtained lattice parameters are shown in table 1.

It is very interesting that the cell volume of the samples decreases with the increase of Ta. According to ionic radius and electronegativity, Ta^{5+} should replace Ti^{4+} and occupy the B site. The ionic radius of Ta^{5+} ($r = 0.64$ Å, CN6) is bigger than Ti^{4+} ($r = 0.605$ Å, CN6), normally,

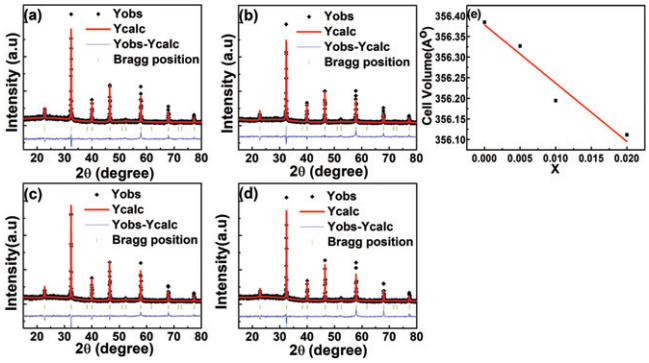

Fig. 1: Rietveld refinement of XRD patterns for $(1-x)$ (0.94BNT-0.06BT)-xTa ceramics using ($R3c$ space group) for (a) $x = 0.00$, (b) $x = 0.005$, (c) $x = 0.01$, (d) $x = 0.02$. (e) The cell volume as a function of x.

Table 1: Lattice parameters of powders with different amounts of Ta addition.

x	a (Å)	b (Å)	c (Å)	V (Å^3)
0	5.5177	5.5177	13.5166	356.385
0.005	5.5174	5.5174	13.5162	356.327
0.01	5.5170	5.5170	13.5130	356.195
0.02	5.5160	5.5160	13.5145	356.112

the cell volume should increase with the increase of the content of Ta_2O_5. However, as shown in fig. 1(e), it shows an opposite variation. The contradiction could be attributed to the defect compensation mechanism [22]. It is known that the volatilization of Bi and Na produces oxygen vacancies. The defect compensation should be

$$\frac{1}{2}\mathrm{Bi_{Bi}} \rightarrow \frac{1}{2}\mathrm{Bi} + \frac{1}{2}V''_{\mathrm{Bi}} + \frac{3}{2}h^{\cdot}, \quad (1)$$

$$\frac{1}{2}\mathrm{Na_{Na}} \rightarrow \frac{1}{2}\mathrm{Na} + \frac{1}{2}V'_{\mathrm{Na}} + \frac{1}{2}h^{\cdot}, \quad (2)$$

$$\mathrm{O_O} \rightarrow \frac{1}{2}\mathrm{O_O} + V^{\cdot\cdot}_{\mathrm{O}} + 2e'. \quad (3)$$

When Ta_2O_5 is introduced into the 0.94BNT-0.06BT system, electron compensation could occur to avoid the formation of oxygen vacancies. With Ta increasing, A-site vacancy compensation would be induced, which gives rise to increasing rather than decreasing the cell volume. As a result, the defect compensation should be

$$\mathrm{Ta} \rightarrow \mathrm{Ta^{\cdot}_{Ti}} + e', \quad (4)$$

$$\mathrm{Ta} \rightarrow \mathrm{Ta^{\cdot}_{Ti}} + V'_{\mathrm{Na}}, \quad (5)$$

$$\mathrm{Ta} \rightarrow \mathrm{Ta^{\cdot}_{Ti}} + \frac{1}{3}V'''_{\mathrm{Bi}}. \quad (6)$$

It is known that the local structure plays an important role in the electrical properties of 0.94BNT-0.06BT ceramics. The change of cell volume would give rise to a lattice distortion and then effect the local structure. The

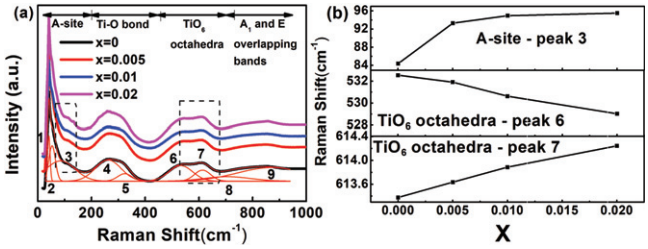

Fig. 2: (a) Raman spectra of $(1-x)$(0.94BNT-0.06BT)-xTa ceramics powders at room temperature with compositions $x = 0.00$, 0.005, 0.01 and 0.02. The red solid lines are deconvoluted by the Gaussian function. (b) Peak positions of $(1-x)$(0.94BNT-0.06BT)-xTa ceramics ($x = 0.00$, 0.005, 0.01 and 0.02).

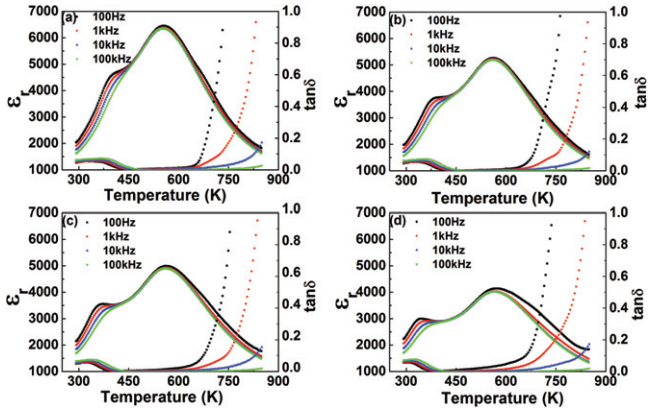

Fig. 3: Temperature dependence of dielectric constant for $(1-x)$(0.94BNT-0.06BT)-xTa ceramics at various frequencies (a) $x = 0.00$, (b) $x = 0.005$, (c) $x = 0.01$, (d) $x = 0.02$.

Raman spectroscopy was employed to identify the local structure of 0.94BNT-0.06BT system. Raman spectra of the ceramics with various Ta are shown in fig. 2. Spectral deconvolution was carried out according to the Gaussian modes [23,24]. It can be observed that there are four main regions in the spectrum: 1) the wavenumber of $\leq$200 cm^{-1} modes are related to the A-site vibration of perovskite oxides; 2) the 200–450 cm^{-1} modes associate with the Ti-O vibration; 3) the 450–700 cm^{-1} modes associate with the vibrations of the TiO_6 octahedra; 4) the high-frequency region above 700 cm^{-1} modes are related to A_1 (longitudinal optical) and E (longitudinal optical) overlapping bands [25]. The Raman band in the peak 3 (marked with dotted line in fig. 2(a)) originating from Bi/Na/Ba-O vibration shifts to higher wavenumber, indicates that the bonds shorten and the binding force increases between them [26]. This is consistent with the XRD refinement results and above-mentioned defect compensation mechanism. Two shoulder-feature bands near high-frequency range of 450–650 cm^{-1} (peak 6 and peak 7 marked with dotted line in fig. 2(a)) are attributed to the vibration of the TiO_6 octahedral. The bands gradually widen with the increase of Ta concentration, indicating distortion and more disorder in the 0.94BNT-0.06BT system with the introduction of Ta [27]. As a result, Ta addition has a significant influence on the A-site vibrations and disorder of the local structure, which is consistent with the report on 0.94BNT-0.06BT–based single crystals [28,29].

Temperature dependence of dielectric properties for the $(1-x)$(0.94BNT-0.06BT)-xTa ceramics from room temperature to 600 °C at selected frequencies are presented in fig. 3. There could be two clear dielectric anomalies in the temperature region for all samples. On the one hand, the low-temperature one exhibits a clear frequency dispersion while the high-temperature one is a typical diffuse phase transition. It is interesting that the dielectric permittivity for the high-temperature dielectric anomaly decreases significantly with the increase of Ta concentration. This is consistent with the XRD and Raman results, suggesting the decrease of cell volume and the enhancement of binding force depress the polarization of B-site ions. On the other hand, the low-temperature dielectric anomaly is attributed to the phase transition from ferroelectric ($R3c$) to anti-ferroelectric ($P4bm$), while the high-temperature one is associated with the anti-ferroelectric ($P4bm$) to paraelectric ($Pm\text{-}3m$) phase transition [30,31]. This is a reentrant relaxor behavior because the relaxor appears below a diffuse phase transition. In addition, the dielectric permittivity of the low-temperature anomaly decreases slowly with the increase of Ta concentration. This could be due to the A-site vacancies and thermal evolution of PNRs in the ceramics [32]. A possible mechanism is that the size of PNRs becomes smaller and the coupling between PNRs becomes weaker with the increase of Ta concentration [33]. As a result, the low-temperature phase transition (reentrant relaxor behavior) becomes more and more visible, the "shoulder" in pure 0.94BNT-0.06BT becomes a distinct peak in the sample 0.98 (0.94BNT-0.06BT)-0.02Ta.

In order to understand the influence of Ta on the diffuse phase transition of 0.94BNT-0.06BT, the modified Curie-Weiss law is applied to describe the dielectric behavior [34]

$$\frac{1}{\varepsilon'} - \frac{1}{\varepsilon'_m} = \frac{1}{k(T-T_m)^\gamma}, \tag{7}$$

where ε'_m is the maximum value of the dielectric constant at the transition temperature (T_m) of the dielectric peak, T is the absolute temperature, γ is the degree of diffuseness and k is a constant. It is well known that γ is equal to 1 for normal ferroelectrics and equal to 2 for typical relaxor ferroelectrics. A linear relationship is observed in all the samples above T_m from $\ln(1/\varepsilon_r - 1/\varepsilon_{rmax})$ *vs.* $\ln(T-T_m)$ plots (fig. 4). As shown in table 2, γ is 1.89, 1.9, 1.82 and 1.86, for $x = 0$, $x = 0.005$, $x = 0.01$, and $x = 0.02$, respectively, which indicates a typical diffuse phase transition [35]. However, no obvious difference can be found for γ, suggesting that the diffuse phase behavior has nothing to do with the Ta concentration. Therefore, the dielectric anomaly could be attributed to more than one transition processes.

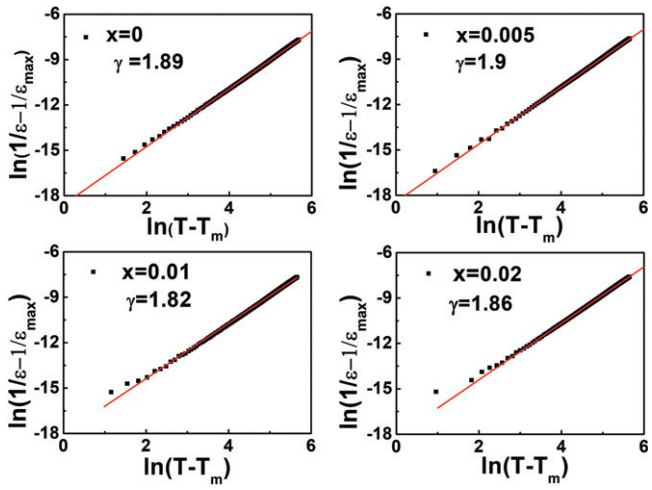

Fig. 4: The $\ln(1/\varepsilon_r - 1/\varepsilon_{rmax})$ *vs.* $\ln(T - T_m)$ for $(1-x)$(0.94BNT-0.06BT)-xTa ceramics with compositions $x = 0$, 0.005. 0.01 and 0.02 at 100 kHz.

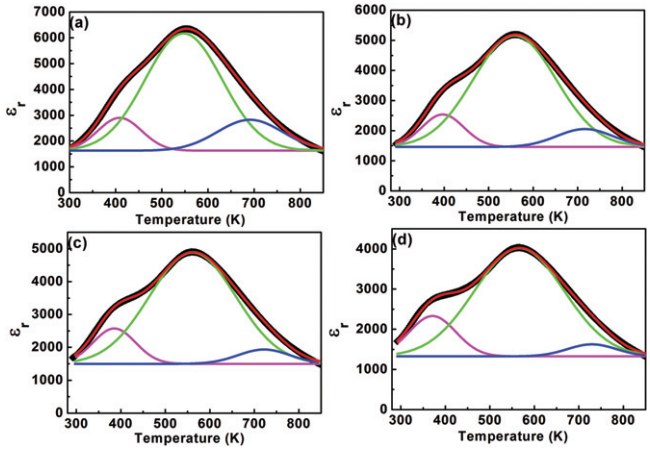

Fig. 5: Temperature dependence of dielectric constant for $(1-x)$(0.94BNT-0.06BT)-xTa ceramics at 100 kHz (a) $x = 0.00$, (b) $x = 0.005$, (c) $x = 0.01$, (d) $x = 0.02$. The red line is fitting based on three Gauss distribution functions. Pink, green and bule lines are deconvoluted be eq. (8) associated with three dielectric relaxation processes.

Table 2: Fitting results by Curie-Weiss law (eq. (7)), Gaussian (eq. (8)).

x	γ	T_o (K)	δ_G (K)
		400.75	108.49
0	1.89	552.23	215.08
		709.44	152.94
		397.00	94.07
0.005	1.90	558.46	186.14
		716.11	126.28
		376.01	111.59
0.01	1.82	562.39	236.23
		727.48	129.35
		350.92	120.42
0.02	1.86	572.33	246.74
		714.39	110.37

Liu *et al.* [36] found that the BNT system includes three relaxation processes in a broad temperature region according to the ferroelectric properties and relaxation time. Here three Gaussian distribution functions with a mean value T_0 and a standard deviation δ_G [37] were used to deconvolute the temperature dependence of dielectric permittivity at 100 kHz as shown in fig. 5.

$$\frac{\varepsilon_0}{\varepsilon - \varepsilon_\infty} = \exp\left[\frac{(T - T_0)^2}{2\delta_G}\right], \tag{8}$$

where ε_∞ is the contribution from the polarization contributed by electron and ionic displacement; ε_o is a temperature- and frequency-dependent parameter. The fitting parameters are listed in table 2.

The low-temperature dielectric relaxation exhibits a strong frequency dispersion, whereas the mid-temperature and high-temperature ones are obvious diffuse phase transitions without frequency dispersion. The three dielectric relaxations correspond to the thermal evolution of *R*3*c* PNRs, the phase transition from *R*3*c* to *P*4*bm*, and the phase transition from *P*4*bm* to *Pm*-3*m* [38], respectively. The change of δ_G shows the decrease of diffuseness degree of the dielectric peak with the increase of Ta concentration. It provides evidence of a composition-induced diffuse phase transition or a relaxor behavior in the system. The δ_G for the thermal evolution of *R*3*c* PNRs and the phase transition of *R*3*c* to *P*4*bm* increase with the increase of Ta concentration. It suggests that the diffuseness degree of the two dielectric relaxations becomes stronger, which is attributed to the degeneration long-range ferroelectric order and the weaker interaction between polar clusters or PNRs. In contrast, the diffuseness degree of the phase transition from *P*4*bm* to *Pm*-3*m* decreases with the increase of Ta concentration. It can be considered that the A-site vacancies created by the introduction of Ta make the ferroelectric domains of *P*4*bm* phase much closer to cubic symmetry.

The low-temperature frequency dispersion of the reentrant relaxor behavior in this system can be described by the Vogel-Fulcher relation [39] as shown in eq. (9). It introduces the concept of "freezing temperature" and reflects the freezing process caused by the interaction between dipoles. The thermal activation-related polarization behavior of PNRs above freezing temperature are also revealed:

$$f = f_0 \exp\left(-\frac{E_a}{k_B\,(T_m - T_f)}\right), \tag{9}$$

where f is probing frequency, f_0 is the relaxation frequency of dipoles, E_a is the activation energy, T_f is the freezing temperature, T_m is the temperature

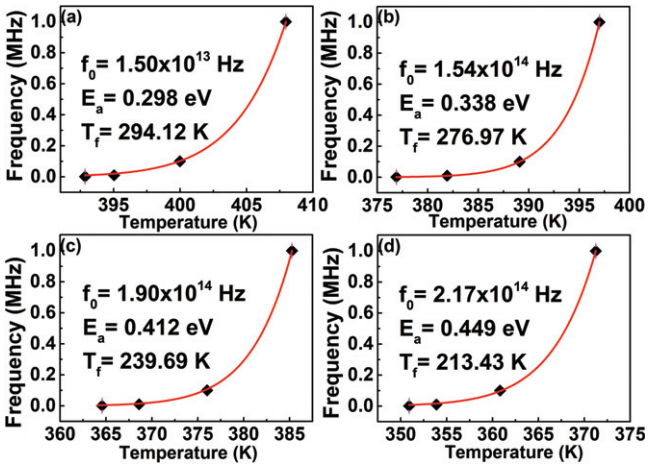

Fig. 6: Vogel-Fulcher fittings of frequency dependence of $T_{\max}$ for $(1-x)$(0.94BNT-0.06BT)-xTa ceramics (a) $x = 0.00$, (b) $x = 0.005$, (c) $x = 0.01$, (d) $x = 0.02$. The red solid line is the Vogel-Fulcher law fitting.

Table 3: Fitting results by Vogel-Fulcher (eq. (9)).

x	f_0 (Hz)	T_f (K)	E_a (eV)
0	1.50×10^{13}	294.12	0.298
0.005	1.54×10^{14}	276.97	0.338
0.01	1.90×10^{14}	239.69	0.412
0.02	2.17×10^{14}	213.43	0.449

corresponding to the maximum relative dielectric constant, and k_B is the Boltzmann constant. The temperature dependence of relaxation frequency for the low-temperature anomaly fitted by eq. (9) are shown in fig. 6. The relaxation time, activation energy and freezing temperature are listed in table 3. The T_f is 294.12 K, 276.97 K, 239.69 K, and 213.43 K, for $x = 0$, $x = 0.005$, $x = 0.01$ and $x = 0.02$, respectively. The freezing temperature decreases with the increase of Ta concentration. The E_a is 0.298 eV, 0.338 eV, 0.412 eV and 0.449 eV, for $x = 0$, $x = 0.005$, $x = 0.01$ and $x = 0.02$, respectively, which suggests that the coupling between polar clusters becomes weaker with the increase of Ta concentration. This is in agreement with the Gaussian distribution results. The substitution of Ti by the bigger-size Ta gives rise to isolated and frustrated polar clusters in the 0.94BNT-0.06BT matrix. The coupling between the neighboring clusters becomes very weak. In addition, the change of E_a may associate with oxygen vacancies [40,41] and A-site ions [42–44]. According to eqs. (1)–(6), Bi/Na vacancies and oxygen vacancies are generated through the loss of a small amount of Bi_2O_3/Na_2O during sintering at high temperature. The loss is also very small and difficult to quantify [45,46]. However, small content of Ta doping as a donor compensates the charged Bi/Na vacancies as

$$2\mathrm{Bi}_{\mathrm{Bi}} + 2\mathrm{Na}_{\mathrm{Na}} + 4\mathrm{O}_{\mathrm{O}} + 3\mathrm{Ta}_2\mathrm{O}_5 \rightarrow \mathrm{Bi}_2\mathrm{O}_3 + \mathrm{Na}_2\mathrm{O} + 2\,\mathrm{V}''_{\mathrm{Bi}} + 6\mathrm{Ta}^{\cdot}_{\mathrm{Ti}} + 15\mathrm{O}_{\mathrm{O}}. \quad (10)$$

As a result, the introduction of Ta restricts the creation of oxygen vacancies and increases the concentration A-site vacancies for further increasing of Ta. This limits the concentration of oxygen vacancies and increases the concentration A-site vacancies, which weaken the ability to obtain the metastable long-range dipole ordering in the ceramics [47]. Meanwhile, because the off-center displacement of Bi gives important contribution to the polarization in the system, the A-site vacancies lead to the decrease of dielectric permittivity of the system.

In summary, the temperature dependence of the dielectric constant of 0.94BNT-0.06BT ceramics can be divided into three dielectric anomalies. The low-temperature anomaly is induced by the evolution of rhombohedral PNRs and exhibits a reentrant relaxor behavior. The coupling between polar clusters becomes weaker with the increase of Ta concentration due to the Ta ions destroy long-range ferroelectric order and decreases the polarization of octahedra by shrinking cell volume. The mid-temperature anomaly is related to the phase transition from rhombohedral to tetragonal. The local lattice distortion and A-site vacancies induced by Ta introduction make dielectric relaxation stronger. The high-temperature dielectric anomaly associates with the phase transition from tetragonal to cubic. The dielectric relaxation becomes weaker with the increase of Ta concentration, which is attributed to A-site vacancies.

Conclusions. – The $(1-x)(0.94Bi_{0.5}Na_{0.5}TiO_3$-$0.06BaTiO_3)$-$x$Ta ($x = 0.00$–$0.02$) ceramics were prepared by the traditional solid sintering method. The average structure of the samples exhibits rhombohedral structure with $R3c$ space group. The cell volume decreases with the increase of Ta concentration. A dramatic defect compensation mechanism was proposed in the system. The oxygen vacancies are restricted while the A-site vacancies increase with the increase of Ta concentration, which confirmed by the Rietveld refinement and Raman spectroscopy. The temperature dependence of dielectric constant includes three dielectric anomalies. The low temperature shows a reentrant relaxor behavior while the others are diffuse phase transition. All the dielectric peaks are suppressed and shift to low temperature with the increase of Ta concentration, which associates with substitution of Ti^{4+} by the bigger-size Ta^{5+} ion. The low-temperature dielectric anomaly can be described by the V-F law. The increased activation energy suggests that the coupling between PNRs or polar clusters becomes weaker due to the shrinking unit cell and local isolated clusters. The high-temperature anomaly is related to the phase transition from tetragonal to cubic which associates with the concentration of A-site vacancies.

* * *

This work was financially supported by the Natural Science Foundation of China (Grant No. 11564010), the Natural Science Foundation of Guangxi (Grant Nos. AA138162, and AA294014), High Level Innovation Team and Outstanding Scholar Program of Guangxi Institutes.

REFERENCES

[1] Park S. E. and Shrout T. R., *J. Appl. Phys.*, **82** (1997) 1804.
[2] Cross L. E., *Ferroelectrics*, **151** (1994) 305.
[3] Chiang Y. M., Farry G. W. and Soukhojak A. N., *Appl. Phys. Lett.*, **73** (1998) 3683.
[4] Fukuchi E., Kimura T., Tani T., Takeuch T. and Saito Y., *J. Am. Ceram. Soc.*, **85** (2002) 1461.
[5] Sahoo B. and Panda P. K., *J. Mater. Sci.*, **42** (2007) 4270.
[6] Yan X. W., Ji H. F., Lam K. H., Chen R. M., Zheng F., Ren W., Zhou Q. and Shung K. K., *IEEE Trans. Ultrason. Ferroelectr. Freq. Control.*, **60** (2013) 1533.
[7] Seifert K. T. P., Jo W. and Rödel J., *J. Am. Ceram. Soc.*, **93** (2010) 1392.
[8] Dai Y. J., Zhang S., Shrout T. R. and Zhang X. W., *J. Am. Ceram. Soc.*, **93** (2010) 1108.
[9] Tan X., Aulbach E., Jo W., Granzow T., Kling J., Marsilius M., Klebbe H. J. and Rödel J., *J. Appl. Phys.*, **106** (2009) 044107.
[10] Danels J. E., Jo W., Rödel J., Honkimäki V. and Jones J. L., *Acta Mater.*, **58** (2010) 2103.
[11] Zhang S. T., Kounga A. B., Jo W., Jamin C., Seifert K., Granzow T., Rödel J. and Damjanovic D., *Adv. Mater.*, **21** (2009) 4716.
[12] Wang X. X., Choy S. H., Tang X. G. and Chan H. L. W., *J. Appl. Phys.*, **97** (2005) 104101.
[13] Yoon M. S., Khansur N. H., Choi B. K., Lee Y. G. and Ur C. S., *Ceram. Int.*, **35** (2009) 3027.
[14] Zhou C. R., Liu X. Y., Li W. Z. and Yuan C. L., *Mater. Res. Bull.*, **44** (2009) 724.
[15] Han F. F., Deng J. M., Liu X. Q., Yan T. X., Ren S. K., Ma X., Liu S. S., Peng B. and Liu J. L., *Ceram. Int.*, **43** (2017) 5564.
[16] Liu L., Fan J. H. Q., Ke S. M. and Chen L. X., *J. Alloys Compd.*, **458** (2008) 504.
[17] Rao M. V. M. and Kao C. F., *Phys. Rev. B: Condens. Matter*, **403** (2008) 3596.
[18] Fu P., Xu Z., Chu R., Li W., Zang G. and Hao J., *Mater. Chem. Phys.*, **124** (2010) 1065.
[19] Ma X., Yin J., Zhou Q., Xue L. and Yan Y., *Ceram. Int.*, **40** (2014) 7007.
[20] Fu P., Xu Z., Chu R., Li W., Zang G. and Hao J., *Mater. Sci. Eng. B*, **167** (2010) 161.
[21] Liu L. J. and Fan H. Q., *J. Electroceram.*, **16** (2006) 293.
[22] Dawson J. A., Chen H. and Tanaka I., *ACS Appl. Mater. Interfaces*, **7** (2015) 1726.
[23] Rout D., Moon K. S., Kang S. J. L. and Kim I. W., *J. Appl. Phys.*, **108** (2010) 084102.
[24] Eerd W. B., Damjanovic D., Klein N., Setter N. and Trodahl J., *Phys. Rev. B*, **82** (2010) 104112.
[25] Schütz D., Deluca M., Krauss W., Feteira A., Jackson T. and Reichmann K., *Adv. Funct. Mater.*, **22** (2010) 2285.
[26] Yang X. X., Zhou Z. F., Wang Y., Li J. W., Guo N. G., Zheng W. T., Peng J. Z. and Sun C. Q., *Chem. Phys. Lett.*, **575** (2013) 86.
[27] Aksel E., Forrester J. S., Foronda H. M., Dittmea R., Damjanovic D. and Jones J. L., *J. Appl. Phys.*, **112** (2012) 054111.
[28] Chen M., Xu Q., Kim B. H., Ahn B. K. and Chen W., *Mater. Res. Bull.*, **43** (2008) 1420.
[29] Hao J. G., Xuaz J., Chu R. Q., Li W., Fu P., Du J. and Li G., *J. Eur. Ceram. Soc.*, **36** (2016) 4003.
[30] Liu L. J., Knapp M., Ehrenberg H., Fang L., Schmitt L. A., Fuess H., Hoelzel M. and Hinterstein M., *J. Appl. Crystallogr.*, **49** (2016) 574.
[31] Liu L. J., Knapp M., Ehrenberg H., Fang L., Fan H. Q., Schmitt L. A., Fuess H., Hoelzel M., Dammak H., Thi M. P. and Hinterstein M., *J. Eur. Ceram. Soc.*, **37** (2017) 1387.
[32] Zang J., Li M., Sinclair D. C., Jo W., Rödel J. and Zhang S., *J. Am. Ceram. Soc.*, **97** (2014) 1523.
[33] Zur. Y. C., Fang X. and Li J., *J. Eur. Ceram. Soc.*, **28** (2008) 871.
[34] Liu L. J., Huang Y. M., Su C. X., Fang L., Wu M. X., Hu C. Z. and Fan H. Q., *Appl. Phys. A.*, **104** (2011) 1047.
[35] Pal V., Dwivedi R. K. and Thakur O. P., *Curr. Appl. Phys.*, **14** (2014) 99.
[36] Liu L. J., Shi D. P., Knapp M., Ehrenberg H., Fang L. and Chen J., *J. Appl. Phys.*, **116** (2014) 184104.
[37] Liu L. J., Shi D. P., Huang Y., Wu S., Chen X., Fang L. and Hu C. Z., *Ferroelectrics*, **432** (2012) 65.
[38] Liu L. J., Ma X., Knapp M., Ehernberg H., Peng B., Fang L. and Hinterstein M., *EPL*, **118** (2017) 47001.
[39] Pirc R. and Blinc R., *Phys. Rev. B*, **76** (2007) 020101.
[40] Kumari R., Ahlawat N., Agarwal A., Sanghi S., Sindhu M. and Rani S., *J. Alloys. Compd.*, **747** (2018) 712.
[41] Steinsvik S., Bugge R., Gionnes J., Tafto J. and Norby T., *Phys. J. Chem. Solids*, **6** (1997) 969.
[42] Praharaj S., Rout D., Anwar S. and Subramanian V., *J. Alloys Compd.*, **706** (2017) 502.
[43] Wang Y., Pu Y. and Zhang P., *J. Alloys Compd.*, **653** (2015) 596.
[44] Dawson J. A., Miller J. A. and Tanaka I., *Chem. Mater.*, **27** (2015) 901.
[45] Li M., Pietrowski M. J., Souza R. A. D., Zhang H., Reaney I. M., Cook S. N., Kilner J. A. and Sinclair D. C., *Nat. Mater.*, **13** (2014) 31.
[46] Li M., Zhang H., Cook S. N., Li L., Kilner J. A., Reaney I. M. and Sinclair D. C., *Chem. Mater.*, **27** (2015) 629.
[47] Ogihara H., Randall C. A. and Trolir M. S., *J. Am. Ceram. Soc.*, **92** (2009) 110.